AD-A139 107 INVESTIGATION OF AERODYNAMICS OF NON AXISYMMETRIC PROJECTILES(U) NEW YORK UNIV WESTBURY ANTONIO FERRI LABS V ZAKKAY ET AL. JAN 84 ARO-19305.2-EG 1/1

UNCLASSIFIED DAAG29-82-K-0075 F/G 20/4 NL

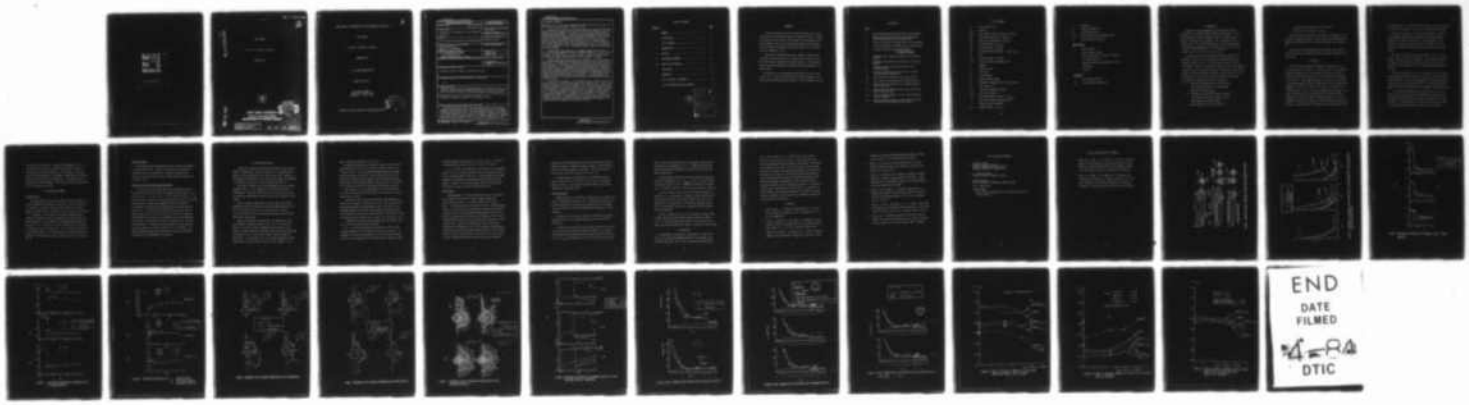

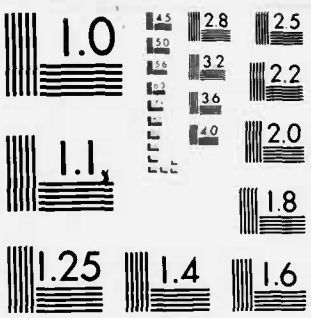

MICROCOPY RESOLUTION TEST CHART
NATIONAL BUREAU OF STANDARDS-1963-A

ARO 19305.2-EG

(2)

AD A139107

FINAL REPORT

V. Zakkay, A. Agnone, B. Prakasam

JANUARY 1984

NEW YORK UNIVERSITY
FACULTY OF ARTS AND SCIENCE
DEPARTMENT OF APPLIED SCIENCE

DTIC FILE COPY

DTIC
ELECTE
MAR 2 0 1984
S D
E

This document has been approved for public release and sale; its distribution is unlimited.

84 03 19 080

2

INVESTIGATION OF AERODYNAMICS OF NON AXISYMMETRIC PROJECTILES

FINAL REPORT

V. Zakkay, A. Agnone, B. Prakasam

JANUARY 1984

U. S. ARMY RESEARCH OFFICE

DAAG 29-82-K-0075

NEW YORK UNIVERSITY
Antonio Ferri Laboratories
Westbury, L.I.,N.Y. 11590

DTIC
ELECTE
MAR 2 0 1984
S D
E

APPROVED FOR PUBLIC RELEASE; DISTRIBUTION UNLIMITED

UNCLASSIFIED
SECURITY CLASSIFICATION OF THIS PAGE (When Data Entered)

REPORT DOCUMENTATION PAGE		READ INSTRUCTIONS BEFORE COMPLETING FORM
1. REPORT NUMBER	2. GOVT ACCESSION NO. AD-A139107	3. RECIPIENT'S CATALOG NUMBER
4. TITLE (and Subtitle) Investigation of Aerodynamics of Non-Axisymmetric Projectiles		5. TYPE OF REPORT & PERIOD COVERED Final Report 3/1/82 - 11/30/83
		6. PERFORMING ORG. REPORT NUMBER
7. AUTHOR(s) Victor Zakkay, Anthony Agnone, and BhadaraPrakasam		8. CONTRACT OR GRANT NUMBER(s) DAAG 29-82-K-0075
9. PERFORMING ORGANIZATION NAME AND ADDRESS New York University Antonio Ferri Laboratories Westbury, L.I.N.Y. 11590		10. PROGRAM ELEMENT, PROJECT, TASK AREA & WORK UNIT NUMBERS
11. CONTROLLING OFFICE NAME AND ADDRESS U. S. Army Research Office Post Office Box 12211 Research Triangle Park, NC 27709		12. REPORT DATE January 1984
		13. NUMBER OF PAGES
14. MONITORING AGENCY NAME & ADDRESS(if different from Controlling Office)		15. SECURITY CLASS. (of this report) Unclassified
		15a. DECLASSIFICATION/DOWNGRADING SCHEDULE

16. DISTRIBUTION STATEMENT (of this Report)

Approved for public release; distribution unlimited.

17. DISTRIBUTION STATEMENT (of the abstract entered in Block 20, if different from Report)

NA

18. SUPPLEMENTARY NOTES

The view, opinions, and/or findings contained in this report are those of the author(s) and should not be construed as an official Department of the Army position, policy, or decision, unless so designated by other documentation.

19. KEY WORDS (Continue on reverse side if necessary and identify by block number)

Aerodynamics, hypersonic, projectiles, experiment, boattails

20. ABSTRACT (Continue on reverse side if necessary and identify by block number)

Recent experiments at subsonic and supersonic speeds, with non-axially symmetric boattailed projectiles, have shown improved drag, pitching moments, and Magnus force characteristics. The non-axisymmetric boattails are formed by cutting the projectile cylindrical body with planes inclined at a small angle (7°) to the projectile's axis so that flat surfaces are created on the boattail, and the base is an inscribed polygon (e.g. a triangle, square, etc.). The flat surfaces increase the boattail lift and decrease the corresponding pitching

DD FORM 1 JAN 73 1473 EDITION OF 1 NOV 65 IS OBSOLETE

UNCLASSIFIED
SECURITY CLASSIFICATION OF THIS PAGE (When Data Entered)

20. ABSTRACT CONTINUED

moments and drag. The present investigation extends the previous research, and the data base into the hypersonic range (M = 6.3).

A second objective of the current investigation was to assess the accuracy and reliability of flow analyses for evaluating the three-dimensional flow field produced by these geometries. The Kutler 3-D, and viscous parabolized Navier Stokes code were evaluated. The analytical results have been compared with detailed surface static pressure and heat transfer measurements, as well as flow field profiles of the impact and static pressures on the conical boattail projectiles, and two non-axisymmetric projectiles: one with triangular cross-section, and the second with a square cross-section. All three configurations were of the same overall length with a slenderness ratio L/D = 7.0, and had a 2.5 calibers tagent ogive nose. Although the expansion angle of the three boattails was identical, i.e., 7°, the individual boattail taper ratio and fineness ratio were different.

The experiments were conducted in a blowdown hypersonic wind tunnel at M = 6.3, and with corresponding free-stream Reynolds number of 1.1×10^7 per foot for angles of attack of 0°, 5°, and 10°. Natural transition occurred on the cylinder. The square boattail was tested at roll angles of 0° and 45°, while the triangular boattail was tested for 0°, 90°, and 180° roll angles.

The measured pressure distributions were integrated to find the axial and normal force coefficients for the complete configuration, and the contribution of the boattails. At zero angle of attack, about 70% of the total drag is due to the ogive nose tip. The boattail accounts for less than 10% of the total axial force coefficient. This is comparable to the base drag and skin friction drag. The triangular boattail configuration produces the smallest drag, compared with the conical and square boattail, since this boattail configuration is longest and has the smallest taper ratio and smallest base area. Nevertheless, the drag reduction over the conical boattail is less than 1%. Similar results are obtained with regard to the normal force coefficient. The present results obtained for M = 6.3, are consistent with the previous results obtained at BRL for supersonic speeds.

The detailed distributions on the windward surfaces, compare very well with the inviscid and viscid analyses for small angles of attack $\alpha \leq 5°$. The inviscid analyses, however, are not in good agreement in regions of strong viscous interactions, and for higher angles of attack $\alpha = 10°$. The PNS code reconciles some of the differences in the viscous interactions regions such as at the sharp cuts on the boattails for angles of attack less than 5°. However, the PNS code fails for $\alpha = 10°$, while the Kutler 3-D code fails on the leeward surfaces at about 135° from the windward most ray, where the rapid expansion is followed by a recompression and cross-flow separation in this region, which is clearly evident in the oil flow tests. The results indicate that inviscid codes may be used to provide guidelines, for possible evaluation of three-dimensional geometric configurations, for drag reduction at low angles of attack.

TABLE OF CONTENTS

Accession For
NTIS GRA&I [X]
DTIC TAB [ ]
Unannounced [ ]
Justification
By
Distribution/
Availability Codes
Dist | Avail and/or Special
A-1

FOREWORD

This report, prepared by New York University Antonio Ferri Laboratories, under U.S. Army Research Contract No. DAAG 29-82-K-0075, presents the research and data analysis from wind tunnel tests conducted on two non-axisymmetric and one conical boattailed projectile configurations. The test program was conducted in the Antonio Ferri M = 6.0 Hypersonic Facility at Westbury, L.I.N.Y.

The Scientific Program Officer was Dr. Robert E. Singleton, and the Technical Program Monitor was Dr. Walter Sturek of the U.S. Army Ballistics Research Laboratories, Aberdeen, Maryland. The parabolized Navier Stokes Code Computations presented herein were performed by Dr. Walter Sturek.

The authors wish to acknowledge the contributions of Mr. Claudio Ferrari, Dr. C.R. Wang, Dr. Wen-Xiong Yang and Akihiko Munakata. This report covers the work performed from March 1, 1982 to November 30, 1983.

ILLUSTRATIONS

FIGURE

LIST OF SYMBOLS

A	cross-sectional area
A_b	base area
A_{cyl}	cross-sectional area of cylinder = $\pi D^2_{cyl}/4$
C_Z	axial force coefficient = $F_Z/q_\infty A_{cyl}$
C_N	normal force coefficient = $N/q_\infty A_{cyl}$
C_D	drag coefficient = $D/q_\infty A_{cyl}$
C_L	lift coefficient = $L/q_\infty A_{cyl}$
C_M	pitching moment coefficient $M/q_\infty A_{cyl} D_{cyl}$
D	drag
D_{cyl}	cylinder diameter - 4 inches
F_Z	axial force due to aerodynamic load
h	enthalpy
l_b	boattail length
L	lift force
M	pitching moment
M_∞	free stream Mach number
N	component of aerodynamic force in y-direction
P	static pressure
$P_{o\infty}$	free stream stagnation pressure
P_{T_2}	local pitot pressure
q_∞	free stream dynamic pressure = $1/2\ \rho_\infty V_\infty$
$\dot{q}$	local heat transfer rate (Btu/ft^2sec)
r	radius or radial coordinate
R_e	Reynolds number = $\rho_\infty V_\infty/\mu_\infty$

T	temperature
T_o	stagnation temperature
V_∞	free stream velocity
x,y,z	body fixed Cartesian coordinate system
Z	axial distance from nose tip

GREEK SYMBOLS

α	angle of attack
γ	ratio of specific heats
θ	cutting phase angle for boattail surfaces = 7°
Φ	roll angle (see Fig. 1)
ϕ	meridional angle from the windward most ray
ρ	mass density
μ	viscosity

SUBSCRIPTS

∞	free stream conditions
cyl	ogive cylinder configuration

I. INTRODUCTION

Substantial range improvements can be obtained by reducing a projectile's drag through improved boattail configurations. It has been shown that non-axially-symmetric boattailed projectiles have a number of advantages over axisymmetric ones. Researchers at BRL, Maryland (Ref. 1), have shown improvements in drag, pitching moments, and Magnus force characteristics, in the speed range up to M = 3 for boattail shapes which do not have axial symmetry.

The present investigation extends the previous research to the hypersonic range (M = 6), for projectiles with three boattail configurations shown in Fig. 1. The investigated boattails include an axi-symmetric (conical) and two non-axi-symmetric (square and triangular) configurations. The latter type boattails are formed by cutting the main projectile cylinder with planes inclined at a small angle (7°), to the projectile axis, so that flat surfaces are created on the boattail. These boattail configurations which were tested are:

a) Square cross-sectioned boattail formed by four cutting planes (90° apart) so that the base becomes an inscribed square.

b) Triangular cross-sectioned boattail formed by three cutting (120° apart) planes so that the base becomes an inscribed triangle.

c) Conical boattail formed by reducing the

cylindrical cross section, so that the boattail portion is like a frustrum of a cone.

Kutler's Inviscid 3-D code (Ref. 2) was used in the analysis. With a view to validate the reliability of the analysis, the predictions were compared with experimental data. Some earlier results were presented in Ref. 3.

The measured and calculated pressure distributions over the projectile surfaces were integrated numerically to obtain aerodynamic force coefficients.

II. ANALYSIS

The inviscid three-dimensional external flow code (Ref. 2), was used for the purpose of analysis. In Kutler's program, the conservation equations (hyperbolic partial differential equations) are solved by finite difference methods marching to successive planes oriented normal to the body axis. The governing equations, in cylindrical coordinates, are normalized between the body and outer boundary (the bow shock) which completely envelopes the influenced flow region. The equations are integrated from an initial data plane to downstream over the body using either a second or third or non-centered finite difference scheme. MacCormack's second order numerical algorithm together with the first method of four possible variations for replacing the space derivatives was used. The bow shock wave is treated as a sharp discontinuity, while

the internal shocks in the flow field are captures by several grid points. A center-plane of symmetry (i.e. zero yaw) is assumed in the analysis.

The grid size consists of 16 radial and 40 meridional (inclusive of the symmetry points) mesh points between the body and an upper boundary which contains the bow shock. A Courant number of 0.9 is specified for stability control and step-size selections. Various clustering at specified peripheral angles can be used to obtain best results.

The analysis has been done for three angles of attack α = 0°, 5° and 10°, with roll angle of zero degrees. Also results were obtained for the square and triangular boattail models with 45° roll angle and 180° roll angle,respectively, for the same above mentioned angles of attack.

Kutler's inviscid code, as it is, can compute flow field for any body configuration without roll effect. Hence, to treat the triangular and square boattail cross-sectioned projectiles, the geometry package of the inviscid code was suitably modified. A sub-routine was also added to the code for the computation of aerodynamic force coefficients.

In an earlier presentation of part of this work (Ref. 3), some mention was made with regard to the computational difficulties that were encountered towards the end of body configuration for 10° angle of attack. In such circumstances, instead of surface entropy remaining constant, entropy jumps were computed indicating numerical

instabilities in the analysis. Sometimes the computation failed. It was found that the results are sensitive to meridional clustering. By changing the clustering parameter, surface entropy in most cases could be maintained constant. Also, moderate improvement in the results were noted particularly on the windward side. The computations were performed on a CDC 6600 computer. The computation time was of the order of 5 to 7 minutes for each case.

III. EXPERIMENTAL PROGRAM

Test Facilities

The experiments for the present investigation were performed in a Mach 6 blowdown-type axisymmetric wind tunnel. The facility consists of a 2000 psia air supply, a capacity heater capable of delivering 900°R air at mass flows up to 60 lb/sec. The test section of the tunnel is 2' in diameter. All the tests of the present experiments were conducted at stagnation pressure and temperature of about 700 psia and 900°R respectively. This resulted in a freestream Reynolds number of the order of 1.1×10^7 per foot. At this condition, natural transition is obtained at about 20" from the nose. This is slightly upstream of the triangular boattail, and is well upstream of the square and conical boattail. Further details of the wind tunnel facility may be found in Ref. 4.

Wind Tunnel Models

Three models have been designed with conical, square,and triangular cross-sectional boattails. Figure 1 gives the detailed dimensions of the models used in the investigation. The details regarding the location of the pressure taps and heat transfer gauges on the model are presented in Ref. 3.

Surface Heat Transfer and Pressure Measurements

The transient thin-skin technique was used to determine the local heat transfer rate from the slope of the temperature-time record. In this technique, the T vs t initial slope is used to compute the heat flux. The test section was evacuated to about the expected free stream static pressure before each test. Pressure and temperature data were recorded on a multi-channel visicorder through galvanometers with response time less than 0.01 sec. Pitot and static pressure profiles were also taken at three locations: the first on the cylindrical portion of the model; the second upstream of the corner of the boattail; and the third downstream of the corner. The flow field profiles are presented in Ref. 3 and are not included here. The measured surface temperature history data were reduced to obtain the local heat transfer rate (q - Btu/Ft^2sec). Local surface pressures measured over the projectile models were normalized with respect to the freestream static pressure.

IV. RESULTS AND DISCUSSION

Surface static pressure data have been presented for three specific boattail configurations. These were plotted as: (1) streamwise distributions in the two meridional rays located in the plane of symmetry, i.e. the windward and leeward most rays; (2) peripheral pressure distributions in the boattail region; and (3) static pressure maps (Ref. 3).

The results presented in this paper complement the results already presented in Ref. 3. Only a sampling of the pressure field data is presented here. Analytical predictions using the Kutler Inviscid code are compared with experimental results to assess the reliability of the analysis.

Figure 2 presents a comparison of surface pressure distribution between the analytical predictions and the experimental results for 0°, 5°, and 10° angles of attack for the ogive portion of the model. It can be seen clearly that the predictions agree well with the experimental data in this region.

Pressure distributions, both analytical and experimental values, on the boattail surfaces are shown in Figs. 3 to 5. For the conical boattail at 0° angle of attack, agreement for the most part of the boattail is good, except near the shoulder, where significant differences are observed (Fig. 3). At 5° and 10° angle of attack, the results compare well. It can be seen in Fig. 4, the results agree well for the square boattail model at 0° and 5° angle of attack. However, at 10°

angle of attack the agreement is not as good.

The leeward side pressure distribution is shown in Fig. 5 for the square boattail (0° roll) and the triangular boattail (180° roll) at 5° angle of attack. The poor agreement between theoretical and experimental values may be attributed to viscous effects due to cross flow separation. Another point of interest is that the predicted pressure distribution for the triangular boattail (180° roll) Fig. 5b, increases rapidly towards the end, while the surface entropy remains constant.

From the above, it can be concluded that the inviscid code does not predict flow field situations accurately on the leeward surfaces for larger angles of attack.

The peripheral static pressure distributions on the boattails at various axial locations are shown in Figs. 6 to 8. The inviscid analysis agrees reasonably well with experimental values in most cases. The difference between the predictions and experiments becomes significant on the leeward side, particularly towards the end of the projectile body. Some parabolized Navier Stokes, Ref. 5, results are also shown in Fig. 8.

A comparison of the pressure distributions along the windward side (Fig. 9) for the different boattails follows:

At α = 0°, the rapid expansion at the shoulder is less for the triangular boattail (0° roll) compared to the square and conical. No expansion occurs for the square boattail (45° roll) along the windward ray since it is an extension of the cylindrical body. However, for the

triangular boattail (180° roll) at α = 0°, and at both α = 5° and 10°, an unexpected pressure decay (curve E) is noted in this region.

At α = 5° and 10°, the expansion at the shoulder for the triangular boattail (0° roll) is almost the same as that of the square and conical. For the triangular boattail (180° roll), a gradual expansion and sudden compression is followed by an expansion over the latter half of the boattail. However, for the square boattail (45° roll) the pressure distribution is similar to that of the cylindrical body.

Heat Transfer

The measurements of the heat transfer were done for the conical and triangular (0° and 180° roll angles) boattail models only. Zakkay and Callahan (Ref. 6) and later Zakkay, Bos, and Jensen (Ref. 7) have shown that the heat transfer rates for turbulent boundary layers in mild adverse pressure gradient are predicted with reasonable accuracy by the flat plate reference enthalpy method (FPRE) of Ref. 8. Based on the conclusions of the previous investigators, the flat plate reference enthalpy method was used for theoretical computation of heat transfer rates. Laminar and turbulent heat transfer rates were computed by the FPRE Method, using the local pressure and temperature distributions and local Mach number obtained from the inviscid analysis. Figure 10 shows the heat transfer rate variation for 0° and 10° angle of attack, respectively,along the projectile with conical boattail.

Comparison with the experimental results shows that laminar conditions prevail on the body. Attempts were made to obtain a turbulent boundary layer by installing roughness on the ogive. Transition occurred on the cylinder at about 20" from the nose tip (Fig. 10).

The heat transfer rate variations for the triangular boattail model (0° and 180° roll) are shown in Figs. 11 and 12 for different angles of attack. It can be seen that laminar boundary layer theory agrees well with measured valves.

Force Coefficients

Another objective of the present investigation was to determine the effect of the boattail geometry on drag. The computed pressure distributions were numerically integrated to evaluate the axial and normal force coefficients and the pitching moment coefficients for all three boattails.

An estimate of the accuracy of the force coefficients computation was made, and an error in computed results was found to be of the order of 4%.

To assess the contribution by the individual boattail to the total drag, the axial force coefficient difference between the particular configuration and the projectile with a straight cylindrical afterbody $\Delta C_Z = C_Z - C_{Z_{CYL}}$ was computed from the results of the inviscid analysis.

The ΔC_Z values from the analytical and experimental results for the three boattails are compared in Fig. 13. Although the differences between experimental and theoretical results are significant, both show a similar trend.

The contribution to the axial force coefficient by the boattail portion of the projectile ($\Delta C_Z + \Delta C_{Z_{base}}$) for 0°, 5°, and 10° angles of attack are shown in Fig. 14. Among the three boattail configurations, a triangular boattail has the maximum drag reduction capability.

In Figs. 13 and 14, ΔC_Z curves for the triangular boattail at a length of 4.77" are also shown. A comparison based on the same boattail length reveals that the triangular boattail does not have the lowest axial force coefficient. This means that the smaller base area of the triangular boattail has a maximum contribution towards total drag reduction.

Finally, a comparison of ΔC_Z's for the boattail surfaces, based on equal base areas, hence different boattail lengths, is made in Fig. 15. Within the computational error all curves are nearly the same, thus indicating base drag influence in the overall drag reduction.

V. CONCLUSIONS

An experimental and analytical investigation of boattail projectile drag reduction was performed. The experiments were conducted at M_∞ = 6.3, and at a free stream Reynolds number based

on the cylinder diameter Re = 3.7 million. Heat transfer measurements were also performed, and the results indicate that the flow field was predominently laminar upstream of the boattail. The results of the analysis indicate that inviscid codes may be used to provide guidelines for possible three-dimensional geometric configurations for the reduction in the drag. The discrepancies between experimental results and theoretical predictions are significant towards the end. Both the experimental and theoretical results indicate that the triangular boattail yields the largest drag reduction. Since the predominant drag of the boattail is the base drag, it is essential for future research, that accurate measurements be performed in the base region of the model in order to have a better comparison between the various boattail configurations.

REFERENCES

1. Platou, Anders, S., "Improved Projectile Boattail", U.S. Army Ballistic Research Laboratories, AIAA J. Spacecraft, Vol. 12, No. 12, December 1975.

2. Kutler, P., Warming, R.F., and Lomax, H., "Computation of Space Shuttle Flowfields Using Noncentered Finite Difference Schemes", AIAA Journal, Vol. 11, No. 2, pp. 196-204, February 1973.

3. Agnone, A.M., Zakkay, V., and Sturek, W.B., "Effects of Boattail Geometry on the Aerodynamics of Hypersonic Projectiles", paper

presented at the AIAA 20th Aerospace Sciences Meeting, Orlando, Florida, January 11-14, 1982, AIAA Paper No. 82-0172.

4. Zakkay, V., "Description of the NYU Wind Tunnel Facilities", New York University Antonio Ferri Laboratory, Bronx, New York, NYU-AA-70-01, January 1970.

5. Schiff, L.B. and Sturek, W.B., "Numerical Simulation of Steady Supersonic Flow Over an Ogive-Cylinder Boattail Body". AIAA 18th Aerospace Sciences Meeting, January 14-16, 1980, Pasadena, California, AIAA Paper No. 80-0066.

6. Zakkay, V. and Callahan, C.G., "Laminar Transitional and Turbulent Heat Transfer to Cone Cylinder Flare Body at Mach 8", Journal of the Aerospace Sciences, Vol. 29, No. 12, December, 1962, pp. 1403-1413.

7. Zakkay, V., Bos, A., and Jensen, P.F., Jr., "Laminar, Transitional and Turbulent Flow with Adverse Pressure Gradient on a Cone flare at Mach 10", AIAA J., Vol. 5, No. 2, February 1967, pp. 201-207.

8. Eckert, E.R.G., "Engineering Relations for Friction and Heat Transfer to Surfaces in High Velocity Flow", Journal of the Aeronautical Sciences, Vol. 22, No. 8, August 1955, pp. 585-586.

LIST OF SCIENTIFIC PERSONNEL

1. Dr. Victor Zakkay
   Professor of Applied Science
   Chairman, Department of Applied Science
   Director, Antonio Ferri Laboratories

2. Dr. Anthony M. Agnone
   Associate Professor of Applied Science

3. Bhadara Prakasam
   Research Assistant, Department of Applied Science

   M.S. - October 1983

   SPECIAL PROJECT:

   "Heat Transfer and Aerodynamics of 3-Dimensional Boattailed Bodies at Mach 6."

LIST OF PAPERS PUBLISHED ON CONTRACT

1. Agnone, A.M., Zakkay, V., and Sturek, W.B., "Effects of Boattail Geometry on the Aerodynamics of Hypersonic Projectiles", paper presented at the AIAA 20th Aerospace Sciences Meeting, January 11-14, 1982, Orlando, Florida. AIAA Paper No. AIAA-82-0172.

2. Zakkay, V., Prakasam, B., and Agnone, A.M., "Analytical and Experimental Investigation of a Boattail Projectile at M = 6.0", paper presented at the 22nd AIAA Aerospace Sciences Meeting, January 9-12, 1984, Reno, Nevada. AIAA Paper No. AIAA-84-0324.

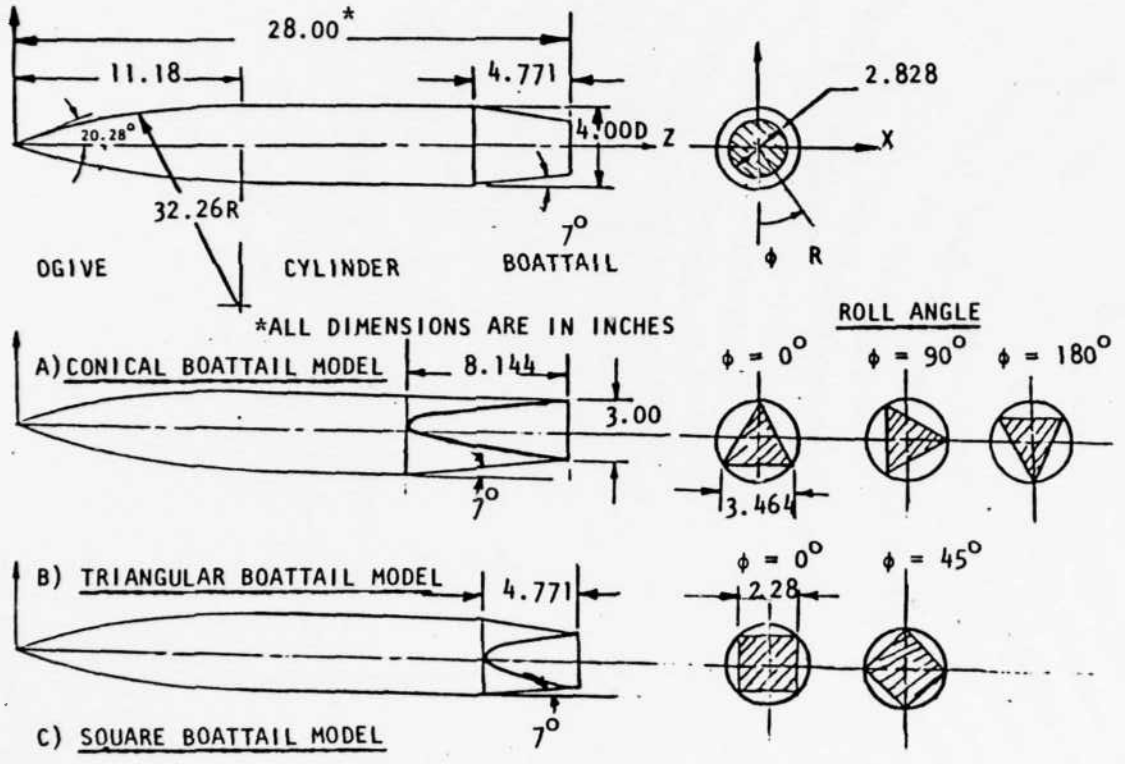

FIGURE 1 BOATTAIL MODEL GEOMETRIES TESTED AND COORDINATE SYSTEM

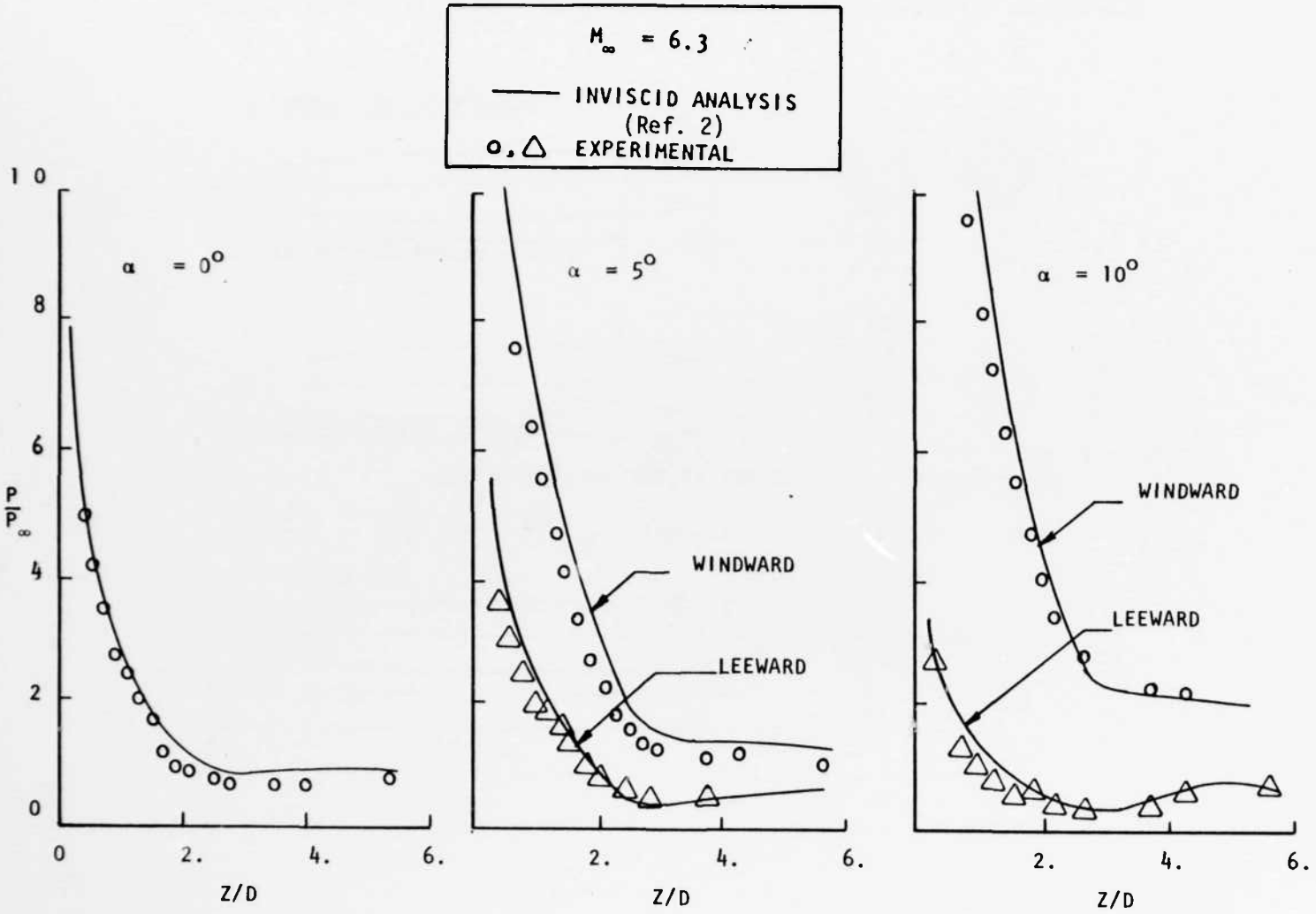

FIGURE 2 STREAMWISE PRESSURE DISTRIBUTIONS ALONG THE WINDWARD MOST AND LEEWARD MOST RAYS ON THE OGIVE BODY

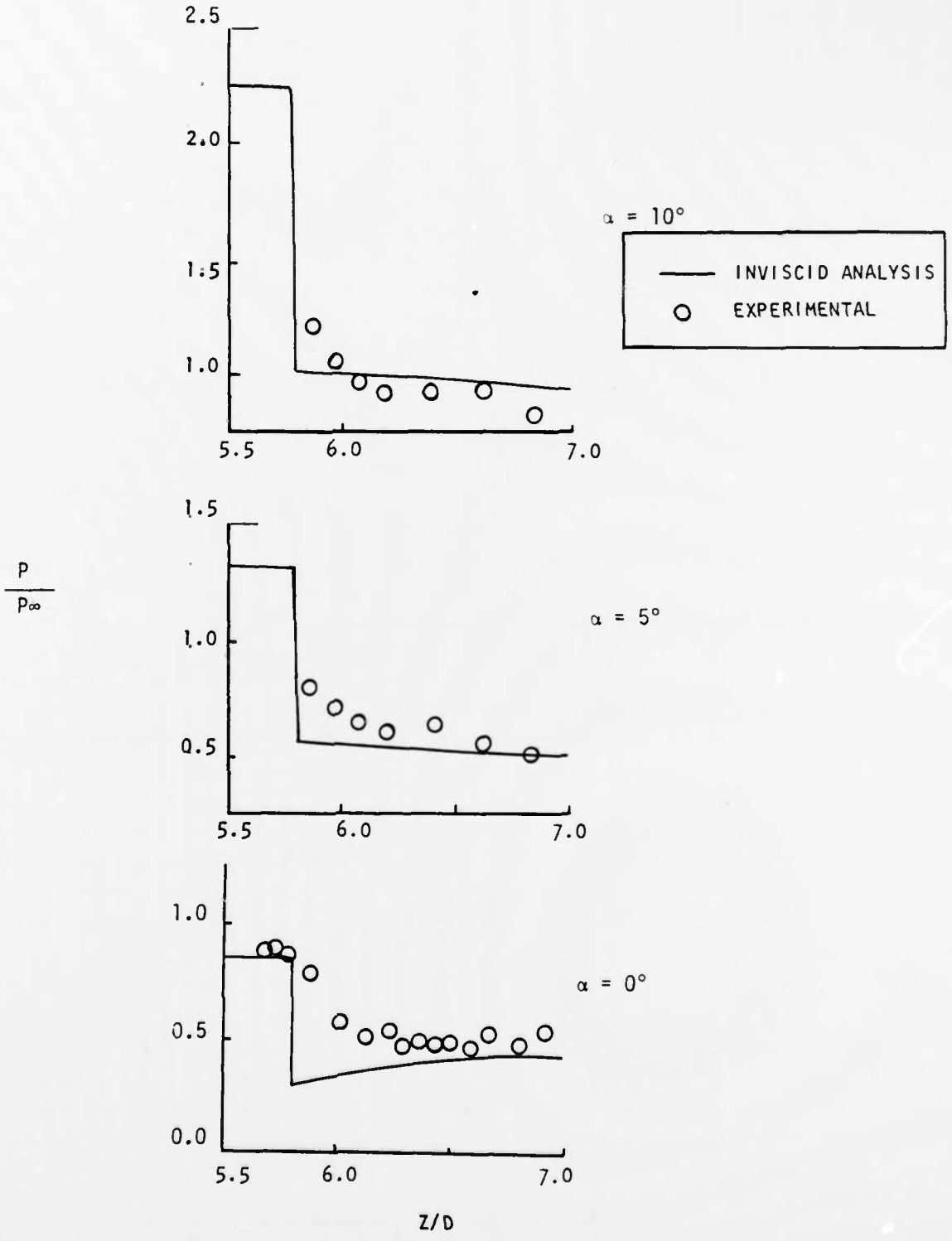

FIGURE 3 PRESSURE DISTRIBUTION ON WINDWARD SIDE OF CONICAL BOATTAIL

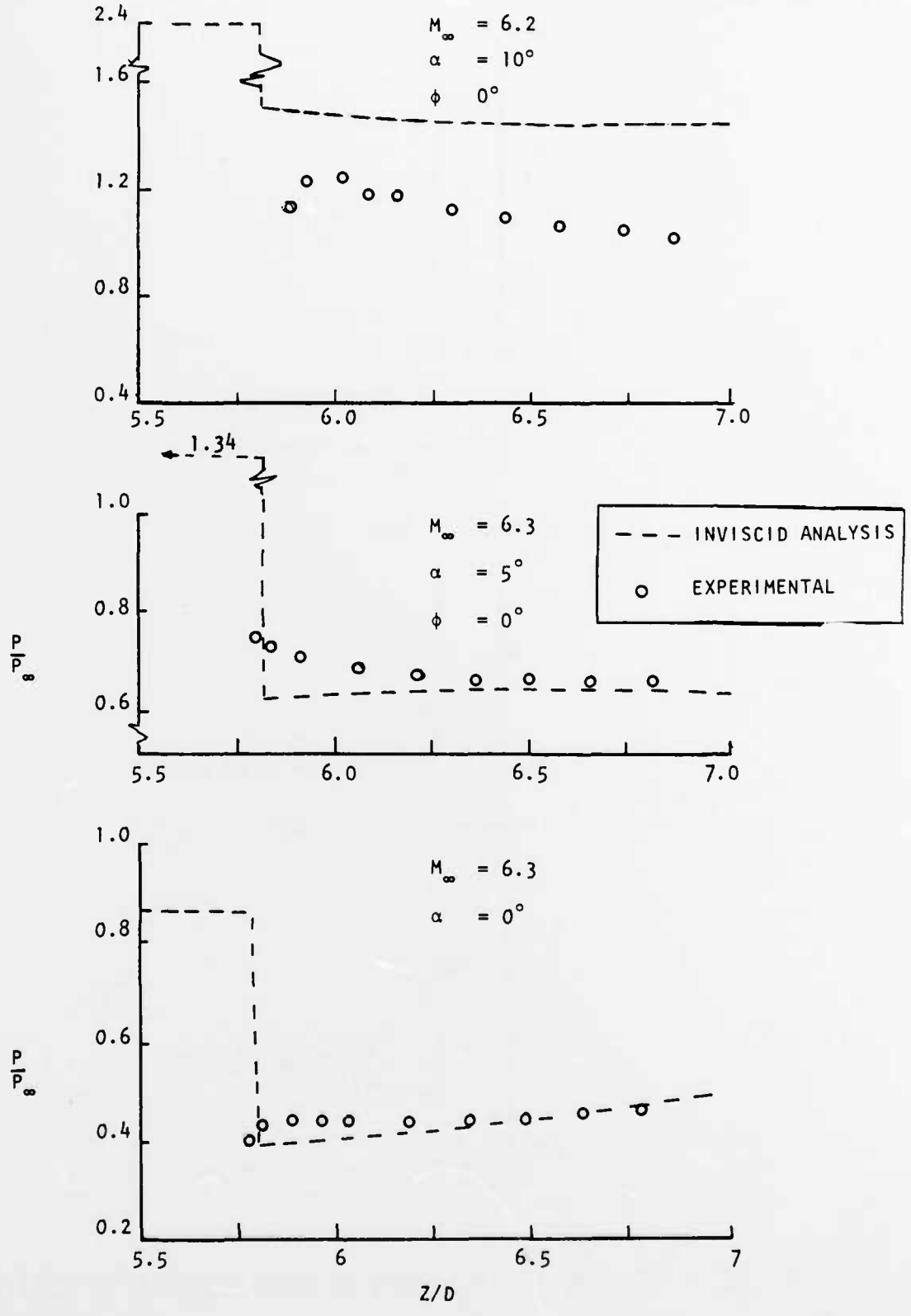

FIGURE 4 PRESSURE DISTRIBUTION ON WINDWARD SIDE OF SQUARE BOATTAIL

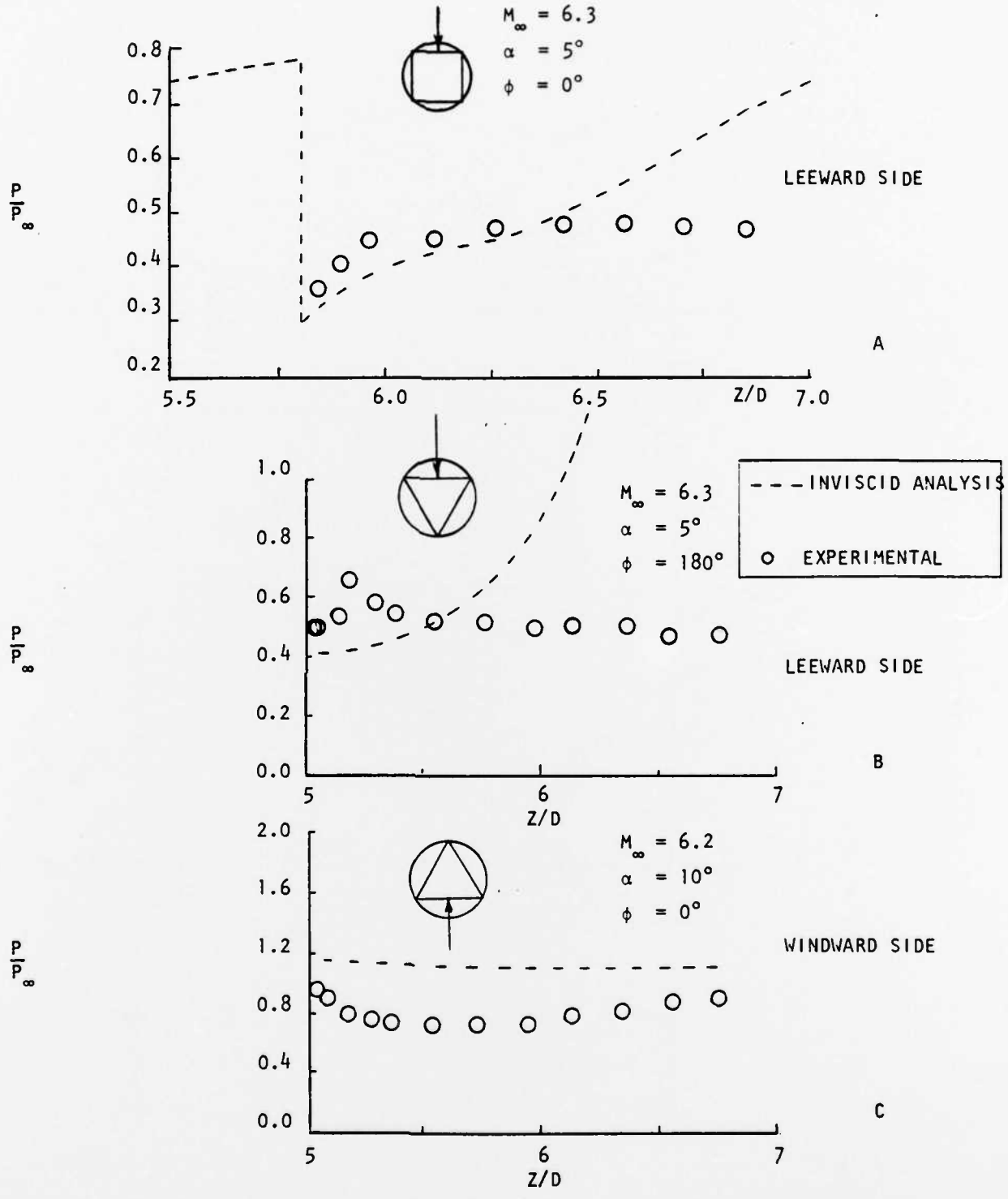

FIGURE 5 PRESSURE DISTRIBUTION ON: A - SQUARE BOATTAIL
B - TRIANGULAR BOATTAIL
C - TRIANGULAR BOATTAIL

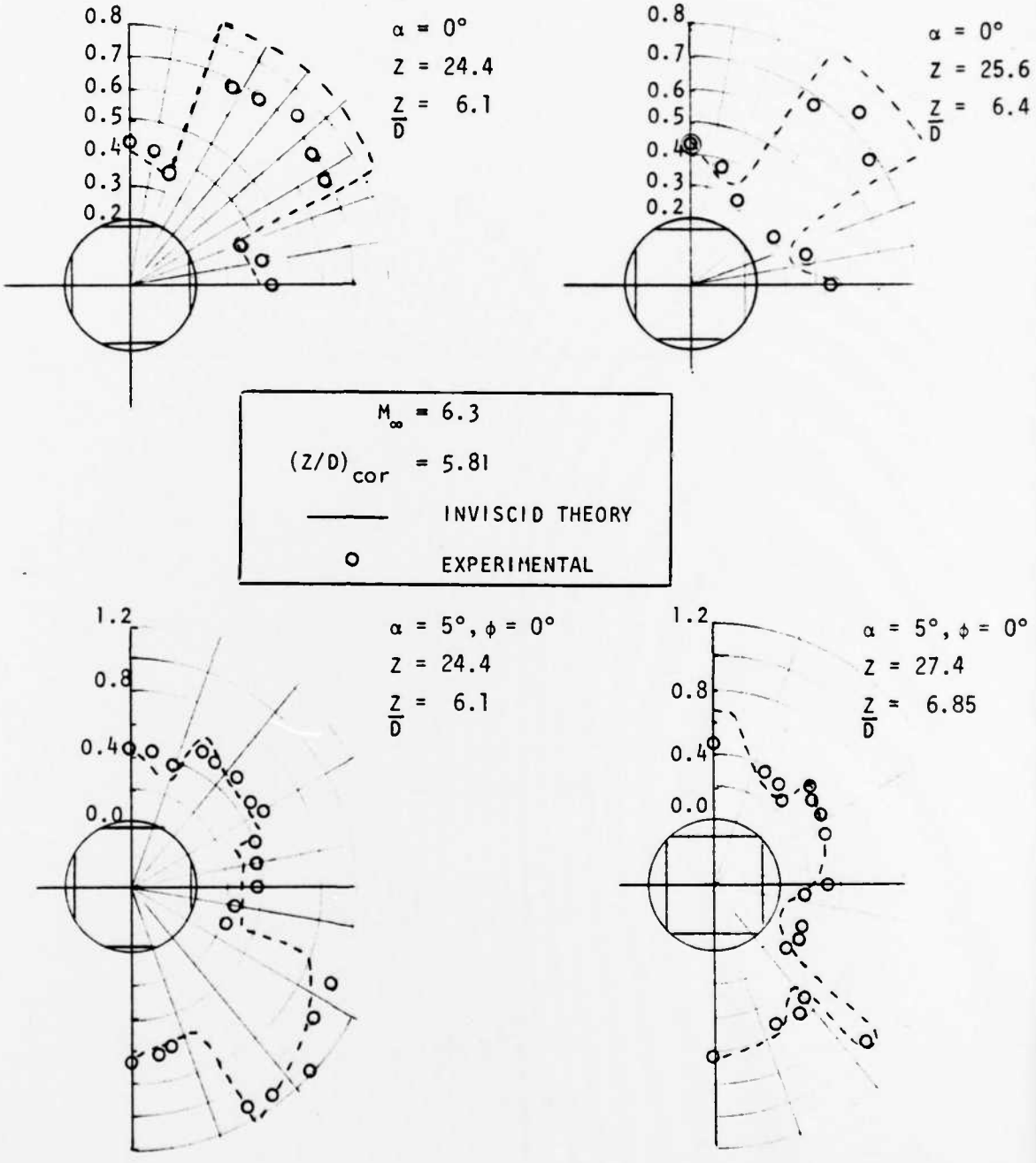

FIGURE 6 PERIPHERAL STATIC PRESSURE DISTRIBUTIONS ON THE SQUARE BOATTAIL

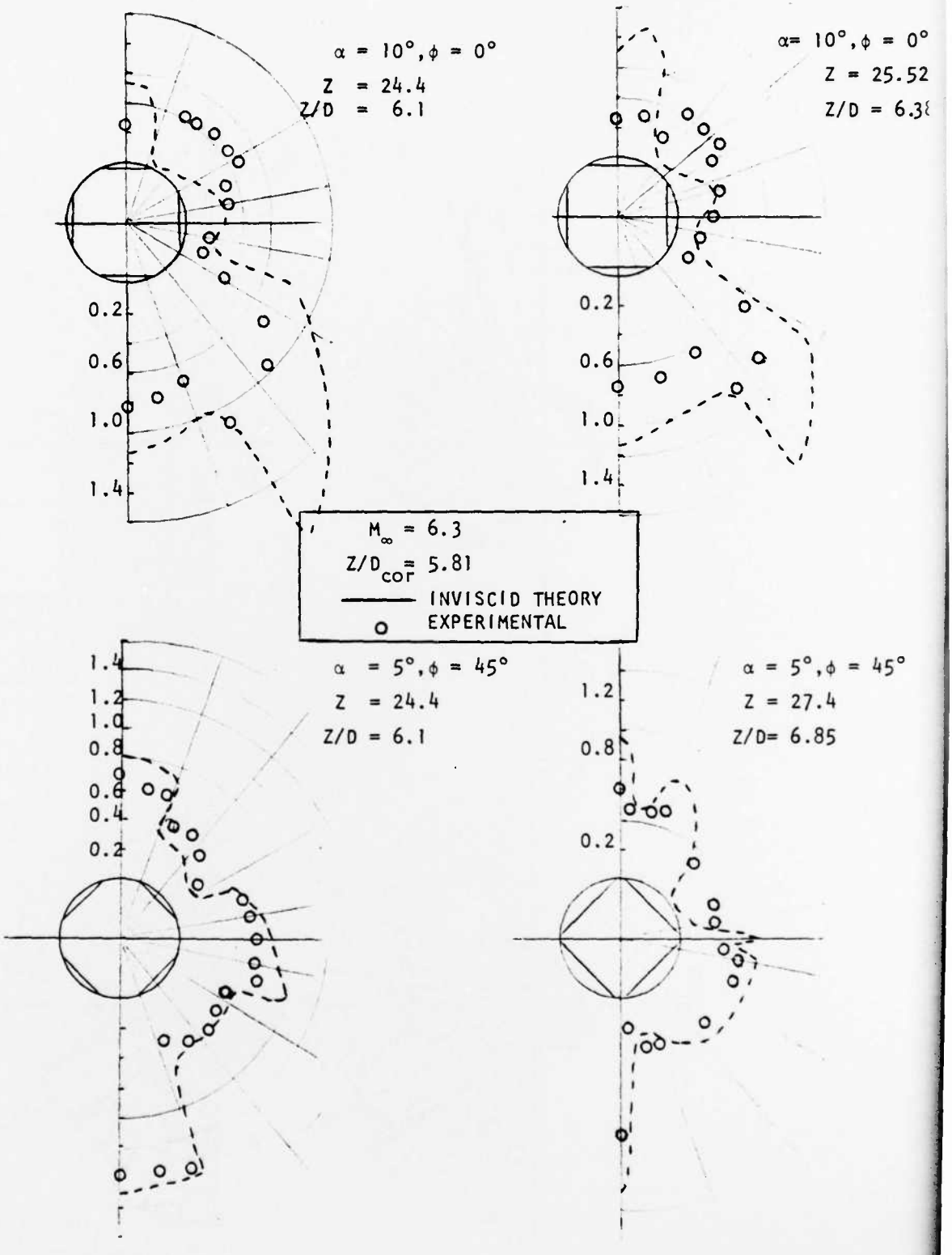

FIGURE 7 PERIPHERAL STATIC PRESSURE DISTRIBUTIONS ON THE SQUARE BOATTAIL

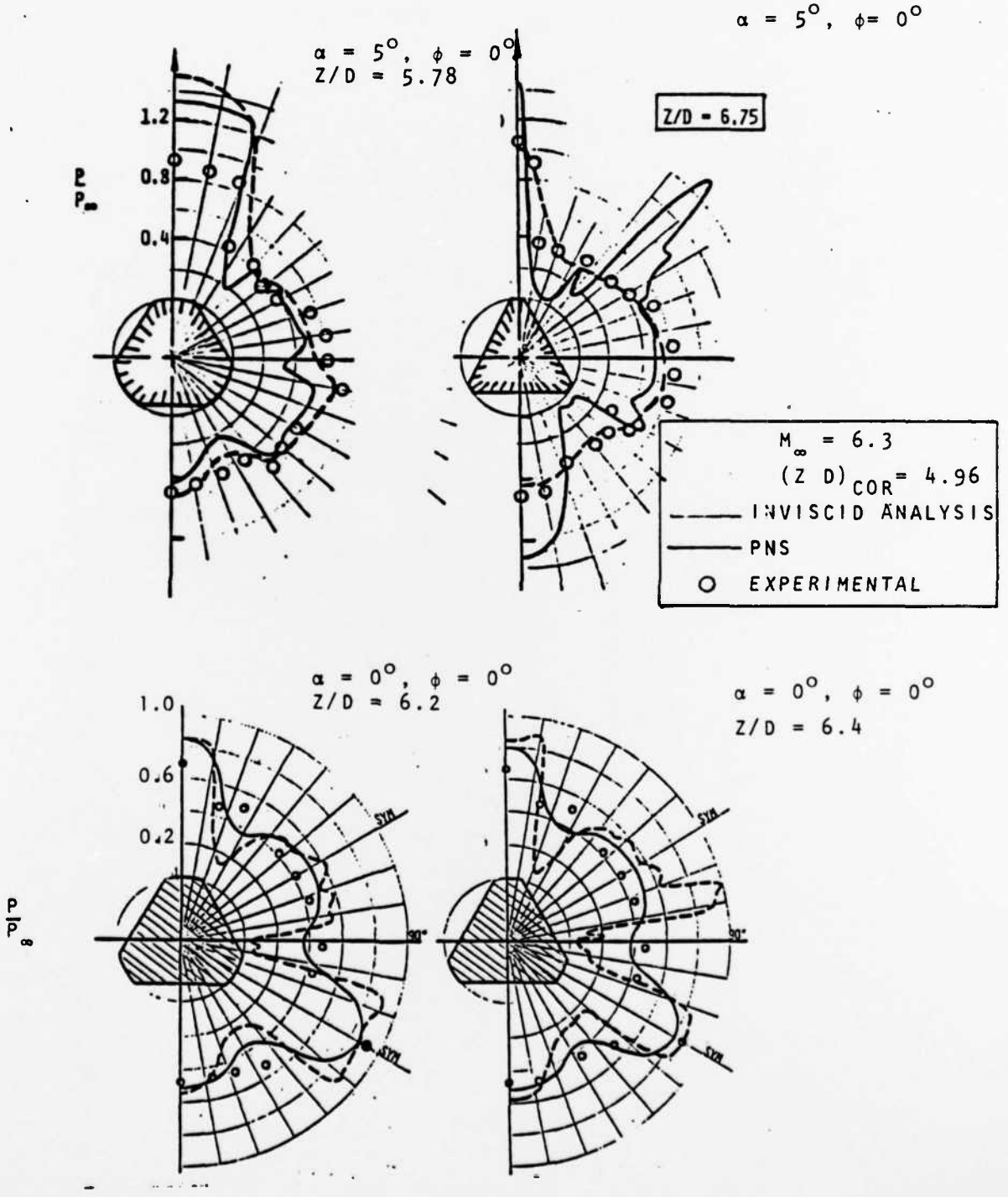

FIGURE 8 PERIPHERAL STATIC PRESSURE DISTRIBUTIONS ON THE TRIANGULAR BOATTAIL

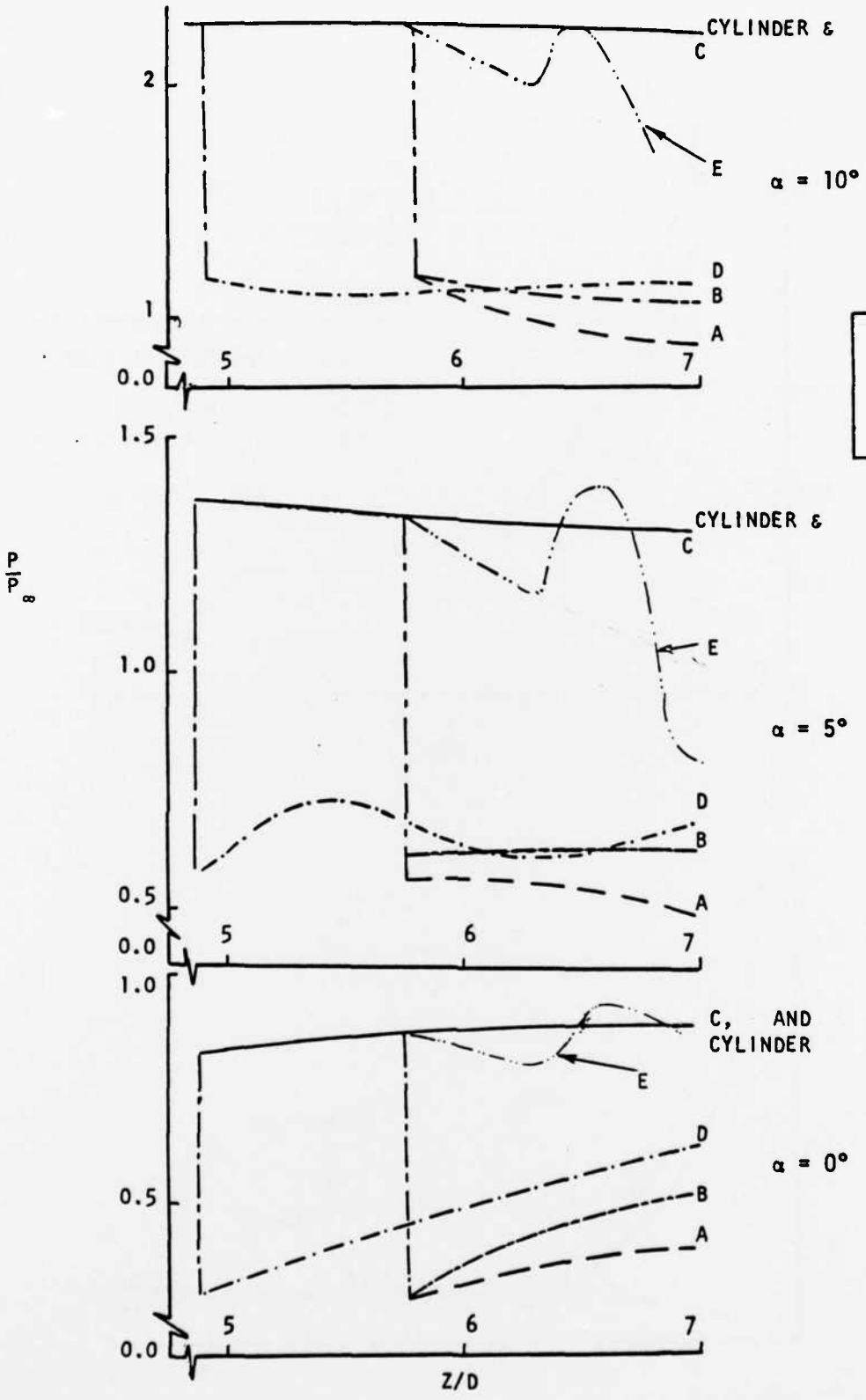

FIGURE 9 PRESSURE DISTRIBUTION ON WINDWARD SIDE (ψ= 0) WITH DIFFERENT BOATTAIL GEOMETRIES

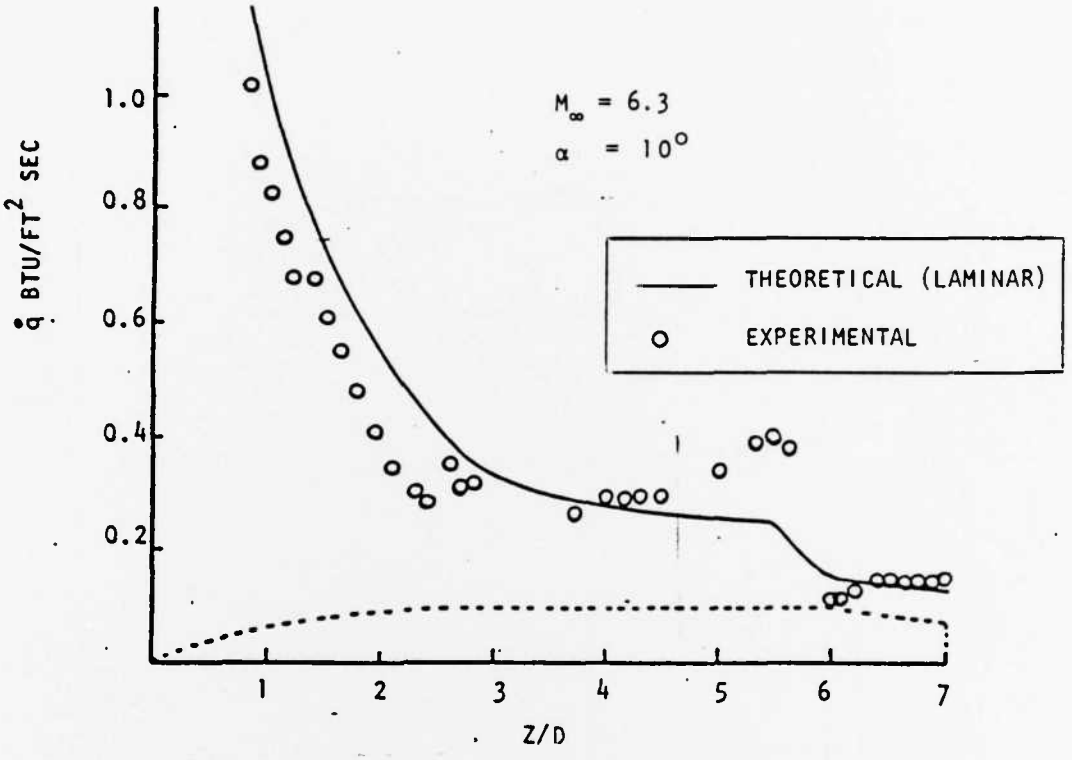

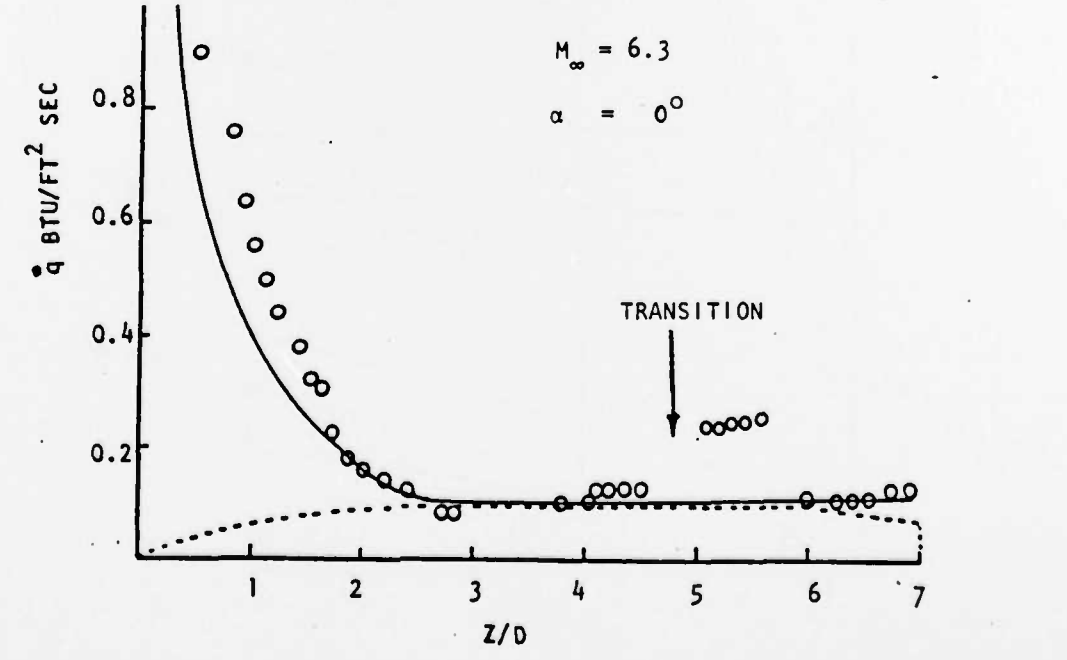

FIGURE 10 HEAT TRANSFER RATE VARIATION WITH CONICAL BOATTAIL

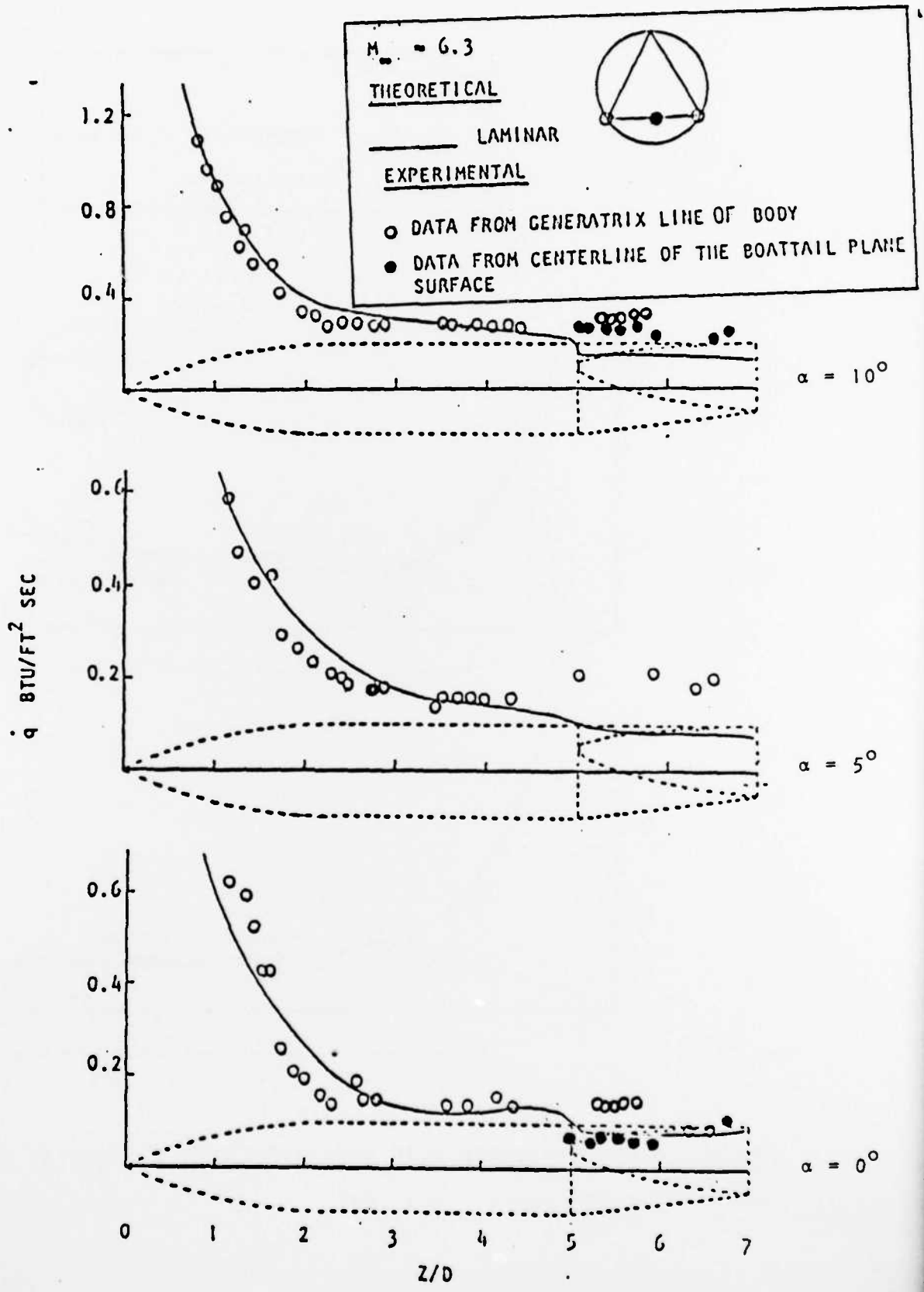

FIGURE 11 HEAT TRANSFER RATE VARIATION WITH TRIANGULAR BOATTAIL

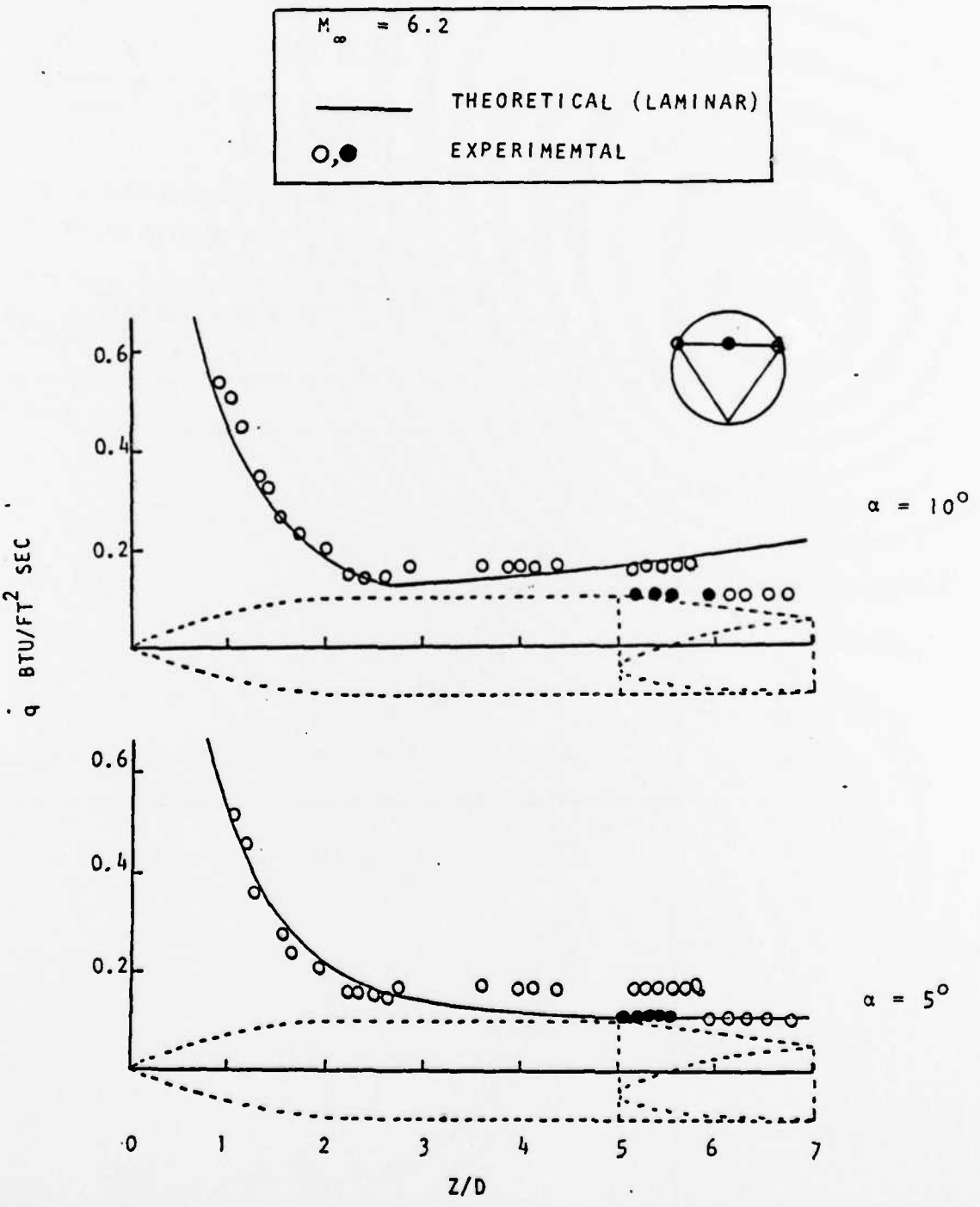

FIGURE 12 HEAT TRANSFER RATE VARIATION WITH TRIANGULAR BOATTAIL (180° ROLL) ψ = 180°

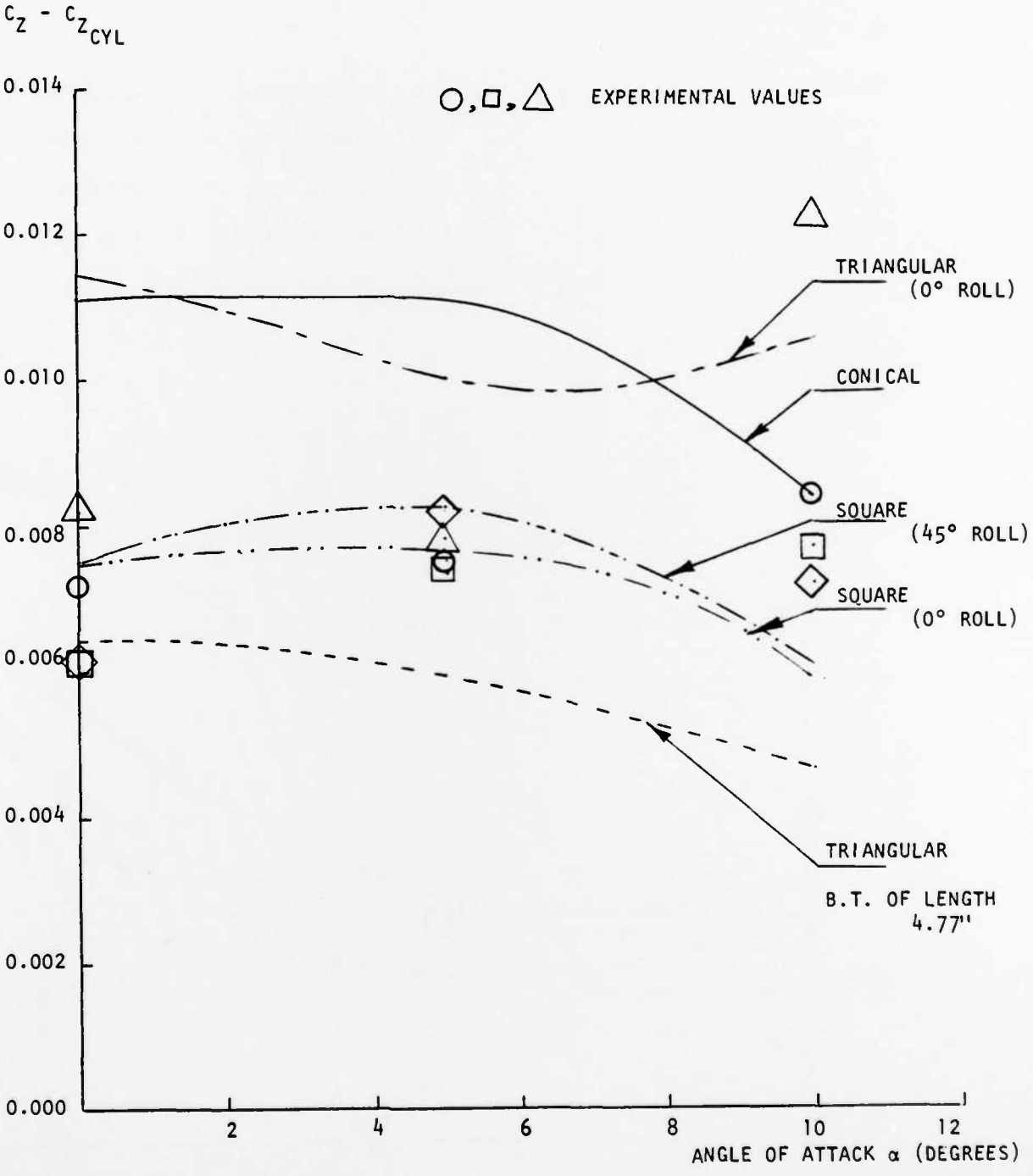

FIGURE 13 EFFECT OF BOATTAIL GEOMETRY ON AXIAL FORCE COEFFICIENT (BASE C_Z NOT INCLUDED)

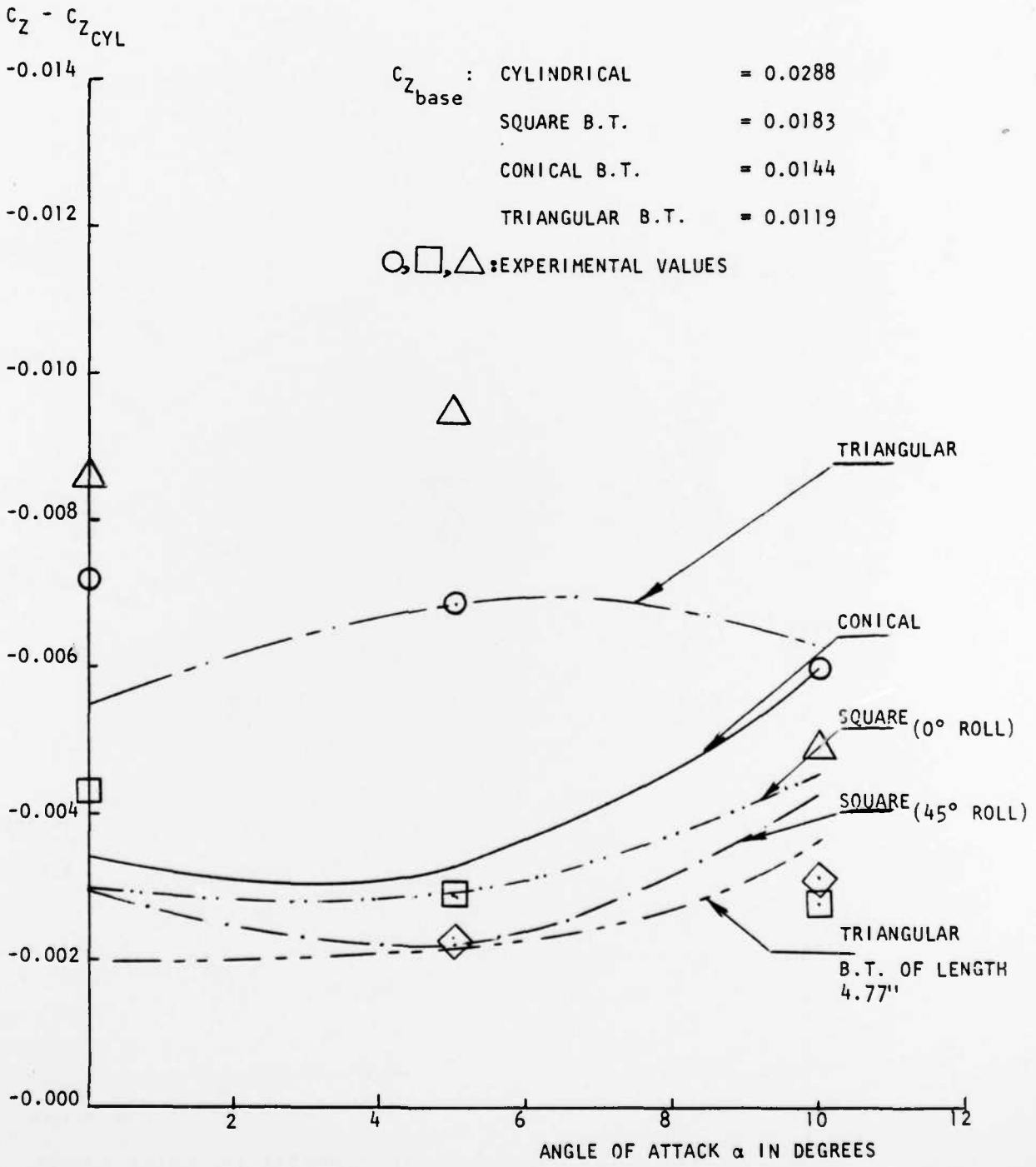

FIGURE 14 EFFECT OF BOATTAIL GEOMETRY ON AXIAL FORCE COEFFICIENT (BASE C_Z INCLUDED)

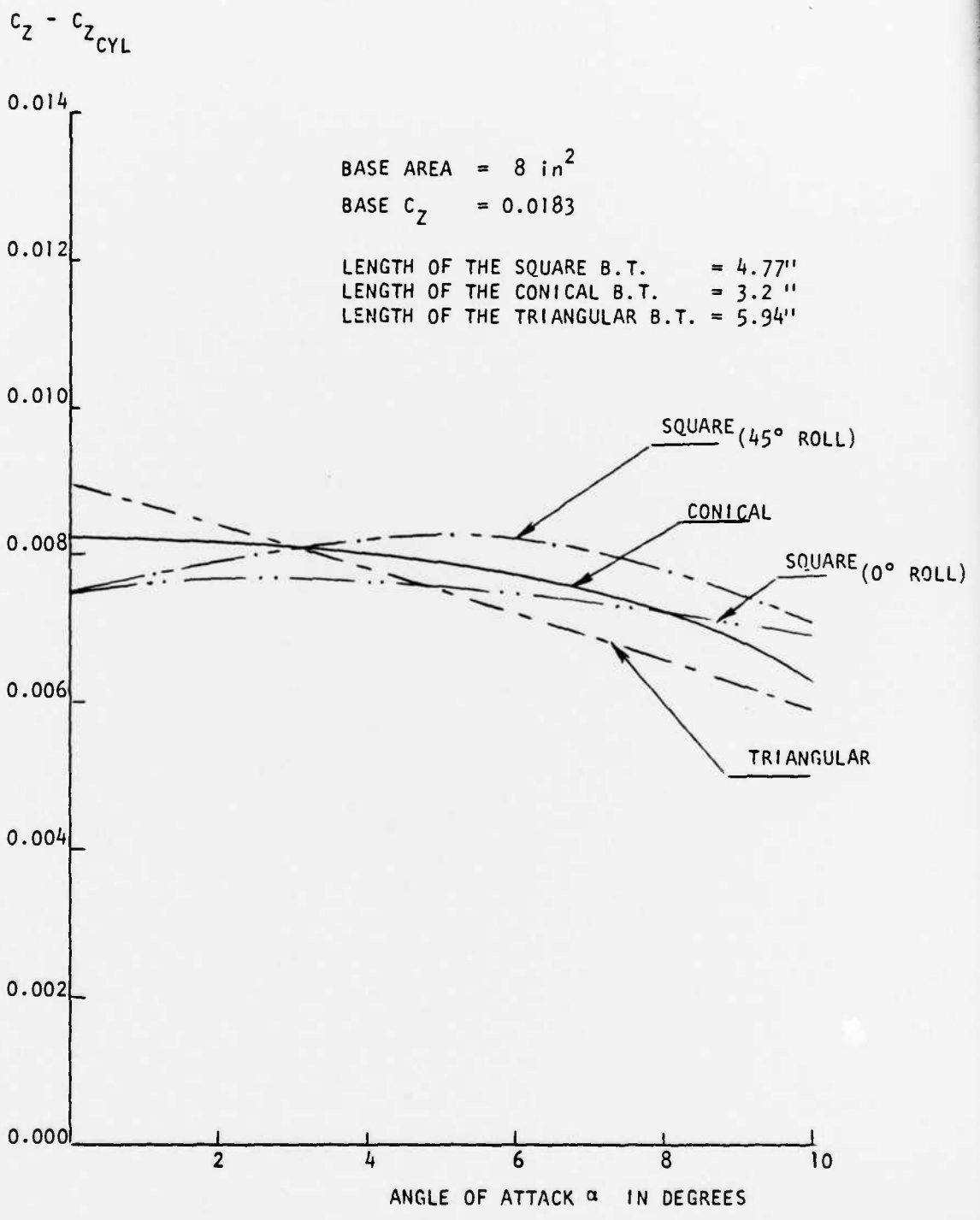

FIGURE 15 EFFECT OF BOATTAIL GEOMETRY ON AXIAL FORCE COEFFICIENT WITH EQUAL BASE AREA (BASE C_Z NOT INCLUDED)


DATE
ILME

BOATTAIL

DTIC